AMERICAN SOCIETY FOR MICROBIOLOGY | Antimicrobial Agents and Chemotherapy®

MECHANISMS OF RESISTANCE

Biochemical and Structural Characterization of CRH-1, a Carbapenemase from *Chromobacterium haemolyticum* Related to KPC β-Lactamases

Florencia Brunetti,[a,b] Barbara Ghiglione,[a,b] Dereje D. Gudeta,[c] Gabriel Gutkind,[a,b] Luca Guardabassi,[d] Sebastián Klinke,[b,e,f] Pablo Power[a,b]

[a]Universidad de Buenos Aires, Facultad de Farmacia y Bioquímica, Instituto de Investigaciones en Bacteriología y Virología Molecular (IBaViM), Buenos Aires, Argentina
[b]Consejo Nacional de Investigaciones Científicas y Técnicas (CONICET), Buenos Aires, Argentina
[c]Division of Microbiology, U.S. Food and Drug Administration, National Center for Toxicological Research, Jefferson, Arkansas, USA
[d]Department of Veterinary and Animal Sciences, Faculty of Health and Medical Sciences, University of Copenhagen, Frederiksberg, Denmark
[e]Fundación Instituto Leloir, Buenos Aires, Argentina
[f]Plataforma Argentina de Biología Estructural y Metabolómica PLABEM, Buenos Aires, Argentina

ABSTRACT KPC-2 is one of the most relevant serine-carbapenemases among the carbapenem-resistant *Enterobacterales*. We previously isolated from the environmental species *Chromobacterium haemolyticum* a class A CRH-1 β-lactamase displaying 69% amino acid sequence identity with KPC-2. The objective of this study was to analyze the kinetic behavior and crystallographic structure of this β-lactamase. Our results showed that CRH-1 can hydrolyze penicillins, cephalosporins (except ceftazidime), and carbapenems with similar efficacy compared to KPC-2. Inhibition kinetics showed that CRH-1 is not well inhibited by clavulanic acid, in contrast to efficient inhibition by avibactam (AVI). The high-resolution crystal of the apoenzyme showed that CRH-1 has a similar folding compared to other class A β-lactamases. The CRH-1/AVI complex showed that AVI adopts a chair conformation, stabilized by hydrogen bonds to Ser70, Ser237, Asn132, and Thr235. Our findings highlight the biochemical and structural similarities of CRH-1 and KPC-2 and the potential clinical impact of this carbapenemase in the event of recruitment by pathogenic bacterial species.

KEYWORDS KPC-2, avibactam, carbapenemases, resistome

The major resistance mechanism in carbapenem-resistant *Enterobacterales* (CRE) is drug hydrolysis by carbapenemases. Among the carbapenemases occurring in clinical bacteria, KPC is one of the most widespread and worrisome families worldwide. From the more than 120 variants in this family, KPC-2 and, to a lesser extent, KPC-3, are by far the most frequently reported. CRE harboring these carbapenemases are typically resistant to other antimicrobial classes, thereby limiting the available therapeutic options (1, 2).

Avibactam (AVI; Fig. 1) is a diazabicyclooctane (DBO) inhibitor that shows efficient inhibition against KPC-2 hydrolytic activity and therefore restores susceptibility when coadministered with partner β-lactams such as ceftazidime (CAZ) as ceftazidime-avibactam (CZA) (3, 4). Since its approval by the FDA in 2015, CZA has been a good treatment option for CRE harboring KPC-2 (5, 6).

Environmental microorganisms carry genes that could potentially confer resistance to different antimicrobial agents, even if they may play a metabolic role rather than being true resistance genes, but when expressed in more efficient genetic environments, they could confer considerable resistance phenotypes (7–9). This reservoir of resistance genes present in environmental microbial communities is known as the

Address correspondence to Pablo Power, ppower@ffyb.uba.ar, or Sebastián Klinke, sklinke@leloir.org.ar.

The authors declare no conflict of interest.

Received 12 January 2023
Returned for modification 20 February 2023
Accepted 10 May 2023
Published 5 June 2023

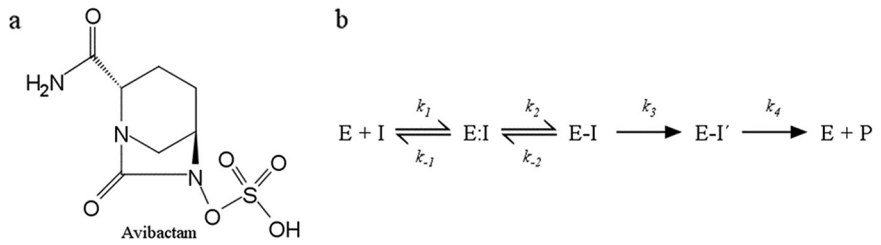

FIG 1 (a) Chemical structure of avibactam (AVI). (b) Kinetic model proposed for the interaction of KPC-2 with AVI (3). In this model, E and I are the enzyme and the AVI, respectively, E:I is the noncovalent complex, and E-I represents the enzyme acylated with AVI. For KPC-2, a slow two-step hydrolytic pathway involving the loss of the sulfate and an imine hydrolysis (E-I′) was proposed, finally leading to the deacylated enzyme and a product (P).

"environmental resistome" (10, 11). Once these genes are mobilized from the resistome into genetic platforms that facilitate their expression and are exposed to higher concentrations of antibiotics, they could reach clinical pathogens in which they may evolve into more specialized variants (7). The most studied example of β-lactamase (*bla*) gene recruitment from environmental microorganisms and subsequent dissemination among clinical isolates is represented by the extended-spectrum β-lactamase (ESBL) CTX-M, for which there is sufficient evidence of it having been recruited from the chromosome of different *Kluyvera* species as preformed cefotaximases (12–15). For other ESBLs such as the PER enzymes, there are some hints that trace their origin back to *Pararheinheimera* (16).

The likely evolutionary origin of the KPC family is still unknown. A recent report described species belonging to the *Chromobacterium* genus carrying genes with high identity with bla_{KPC-2} (17). These genes encode putative β-lactamases named CRP-1 (from *Chromobacterium piscinae*), CRH-1 (from *Chromobacterium haemolyticum*), and CRS-1 (from *Chromobacterium* sp. strain C-61), sharing 76%, 69%, and 70% amino acid identity with KPC-2, respectively. Phylogenetic analysis showed that these *bla* genes are more related to KPC-2 than to other β-lactamases, and when expressed in recombinant *Escherichia coli* clones, they increase MICs for penicillins, cephalosporins, and carbapenems (17).

In this study, we analyzed the kinetic behavior and crystallographic structure of the CRH-1 β-lactamase compared to KPC-2, to explore the role of *Chromobacterium* as a reservoir of close relatives of KPC-2 gene precursors and the potential evolutionary pathway from the resistome to the clinical environment of this carbapenemase.

RESULTS AND DISCUSSION

CRH-1 production in *E. coli* confers increased MIC values to penicillins, cephalosporins, and carbapenems. Antimicrobial susceptibility assays showed that the expression of bla_{CRH-1} in the *E. coli* pM-CRH-1 recombinant clone yielded higher MIC values for most β-lactams tested, carbapenems included, than the *E. coli* pM-KPC-2 clone (Table 1). This effect was less noticeable for ceftazidime and aztreonam. The CRH-1 recombinant clone was also resistant to ampicillin/sulbactam but remained susceptible to ceftazidime-avibactam. Compared to the previous phenotypic profile reported for this β-lactamase (17), the MIC values obtained in our work were higher, possibly due to the differential genetic background used for cloning, resulting in higher protein production.

Under equivalent assay conditions, MIC values obtained for the recombinant clone producing CRH-1 were higher than those observed for the clone harboring bla_{KPC-2}, except for aztreonam and ceftazidime-avibactam. In particular, MICs for imipenem and meropenem were 8-fold higher for CRH-1 than KPC-2.

The MICs values obtained for the environmental *Chromobacterium haemolyticum* DSM19808 strain (from which the bla_{CRH-1} gene used in this study was amplified) show that this isolate is susceptible to imipenem and meropenem (Table 1).

The recombinant *E. coli* clone harboring bla_{CRH-1} showed synergy between imipenem-

TABLE 1 MICs of *E. coli* TOP10F′ recombinant clones and environmental strain *Chromobacterium haemolyticum* DSM19808

	MIC (μg/mL) of:				
Antibiotic	***Chromobacterium haemolyticum* DSM19808**	***E. coli* TOP10F′**	***E. coli* TOP10F′/ pMBLe[a]**	***E. coli* pM-CRH-1**	***E. coli* pM-KPC-2**
Ampicillin	>32	2	2	>2,048	1,024
Ampicillin - sulbactam	>32	2/1	2/1	1,024/512	64/32
Cephalothin	>16	8	8	2,048	256
Ceftriaxone	32	≤0.25	≤0.25	128	8
Ceftazidime	≤1	≤0.25	≤0.25	4	2
Ceftazidime - avibactam	ND[b]	≤0.25/4	≤0.25/4	≤0.25/4	0.5/4
Cefepime	≤4	≤0.25	≤0.25	32	1
Aztreonam	ND	≤0.25	≤0.25	4	16
Imipenem	≤1	≤0.25	≤0.25	16	2
Meropenem	≤1	≤0.25	≤0.25	8	1

[a]*E. coli* clone harboring the empty pMBLe vector.
[b]ND, not determined.

meropenem and boronic acid disks in the double-disk diffusion synergy test (DDST), suggesting similar inhibitory activity by boronic acid compared to that of KPC-2 (18).

CRH-1 displays carbapenemase activity similar to that of KPC-2. To better understand the MIC values due to bla_{CRH-1} expression, we determined and compared the steady-state kinetic parameters for the hydrolysis of different β-lactams for CRH-1 and KPC-2 (Table 2). The results demonstrated that CRH-1 can hydrolyze a broad variety of β-lactams with high hydrolytic efficiency. Compared to the KPC-2 kinetic parameters, CRH-1 showed higher catalytic efficiencies (k_{cat}/K_m) toward ampicillin, piperacillin, and cephalothin, with k_{cat}/K_m values up to 12-fold higher. These differences are explained by the higher apparent affinity (lower K_m) for ampicillin and cephalothin and a higher turnover value (k_{cat}) for piperacillin.

CRH-1 activity toward oxyimino-cephalosporins is represented by a higher hydrolytic efficiency for ceftriaxone (similar k_{cat}/K_m value to KPC-2) in contrast to poor activity toward ceftazidime. Regarding ceftazidime, CRH-1 showed lower K_m than KPC-2, but the turnover value could not be determined due to the lack of detectable hydrolysis under steady-state conditions. This suggests that CAZ is not a good substrate for CRH-1, a kinetic characteristic also related to KPC-2.

Kinetic data for carbapenems confirmed not only that CRH-1 has carbapenemase activity, but also that catalytic efficiencies toward imipenem (IMI) and meropenem (MER) are at least equivalent to those for KPC-2. The CRH-1 k_{cat}/K_m values for IMI and MER were slightly higher than that of KPC-2 (1.6 and 1.4-fold higher, respectively), mainly due to a higher affinity (lower K_m) for both carbapenems.

In general, the kinetic profile described for CRH-1 correlates with the resistance levels conferred by the production of this enzyme in the *E. coli* recombinant clone. However, similar hydrolytic efficiencies for both CRH-1 and KPC-2 were obtained toward ceftriaxone, and to a lesser extent, the carbapenems, which cannot thoroughly explain the higher MICs obtained for CRH-1. Additionally, although KPC-2 exhibits a

TABLE 2 Kinetic parameter comparison of β-lactam hydrolysis

	CRH-1			**KPC-2**		
β-Lactam substrate	**K_m (μM)**	**K_{cat} (s^{-1})**	**K_{cat}/K_m ($\mu M^{-1} \cdot s^{-1}$)**	**K_m (μM)**	**K_{cat} (s^{-1})**	**K_{cat}/K_m ($\mu M^{-1} \cdot s^{-1}$)**
Ampicillin	26 ± 8	71 ± 31	2.7 ± 0.9	537 ± 87	115 ± 8	0.22 ± 0.5
Piperacillin	64 ± 8	167 ± 7	2.61 ± 0.41	97 ± 12	29 ± 1	0.30 ± 0.05
Cephalothin	44 ± 7	79 ± 4	1.8 ± 0.4	159 ± 15	56 ± 2	0.36 ± 0.05
Ceftriaxone	68 ± 7[a]	11 ± 1	0.157 ± 0.005	267 ± 29[a]	52 ± 7	0.194 ± 0.006
Ceftazidime	250 ± 9[a]	ND[b]		1,319 ± 145[a]	0.9 ± 0.1	0.00083 ± 0.00004
Cefepime	369 ± 29[a]	3.5 ± 0.4	0.0095 ± 0.0004	59 ± 5	1.31 ± 0.04	0.022 ± 0.003
Imipenem	19 ± 2	4.00 ± 0.09	0.20 ± 0.03	120 ± 9	15.0 ± 0.4	0.12 ± 0.01
Meropenem	12 ± 2	2.00 ± 0.05	0.13 ± 0.03	31 ± 2	2.85 ± 0.06	0.091 ± 0.009

[a]Parameters were determined with nitrocefin used as the reporter in competitive assays.
[b]ND, not determined because of a lack of detectable hydrolysis under steady-state conditions.

TABLE 3 Inhibition kinetic parameter comparison for avibactam and clavulanic acid

	Avibactam		Clavulanic acid		
β-lactamase	K_{i-app}[a] (μM)	k_2/K (M^{-1} s^{-1})	K_m (μM)	K_{inact} (s^{-1})	K_{inact}/K_m ($\mu M^{-1} \cdot s^{-1}$)
CRH-1	0.400 ± 0.07	32,219 ± 1,933	29.4 ± 1.5	0.0075 ± 0.0005	0.00026 ± 0.00003
KPC-2	0.060 ± 0.004	25,000 ± 19	80 ± 8	0.002 ± 0.0001	0.000025 ± 0.000004

[a]K_{i-app}, apparent affinity constant for inhibition; k_2/K, acylation rate constant.

2-fold higher hydrolytic efficiency toward cefepime compared to CRH-1, this is not reflected in the MIC values. Thus, there is still not a clear explanation for the lack of correlation between some MICs and the kinetic data. Although this could be at least in part attributed to differences in gene expression from the *E. coli* recombinant clones, it deserves further evaluation.

Inhibition of CRH-1 by clavulanate and avibactam. Previous reports described that KPC-2 hydrolyzes clavulanic acid, tazobactam, and sulbactam, resulting in an ineffective inhibition by these inhibitors (19, 20). To study if CRH-1 shares a similar behavior, we performed a kinetic assay to characterize its inhibition by clavulanic acid. The results obtained are shown in Table 3.

The inhibition efficiency (k_{inact}/K_m) of clavulanic acid against CRH-1 was 10-fold higher than that against KPC-2, which is consistent with a higher apparent affinity for this inhibitor (K_m 2.7-fold lower), and the inactivation rate (k_{inact}) was 3.75-fold higher than that against KPC-2. Although CRH-1 appears to be inactivated more efficiently by clavulanic acid than by KPC-2, the k_{inact}/K_m value obtained in this study is still considerably lower than the values reported for other enzymes that are effectively inhibited, such as the ESBLs CTX-M-96 (0.045 $\mu M^{-1} \cdot s^{-1}$) (21) and PER-2 (0.48 $\mu M^{-1} \cdot s^{-1}$) (22). This weaker inhibition by clavulanic acid described for KPC-2 and CRH-1 has not been reported in other class A carbapenemases such as SME-1 (23), IMI-1 (24), and NMC-A (25). The 50% inhibitory concentration (IC_{50}) values reported for BIC-1 (26) and SFC-1 (27) suggest that these enzymes were also weakly inhibited by clavulanic acid.

To this point, we assessed that CRH-1 is ineffectively inhibited by clavulanic acid. To further investigate the interaction of CRH-1 with this inhibitor, we decided to study whether CRH-1 hydrolyzes clavulanic acid as a substrate. Therefore, hydrolysis of clavulanic acid was monitored at 235 nm by mixing an inhibitor concentration five times the K_m and 100 nM enzyme. We observed cleavage of clavulanic acid for KPC-2 (as expected), but also for CRH-1. Since we used an inhibitor concentration 5 times the K_m, the initial rate (v_0) of hydrolysis under this condition was considered to be close to the maximum velocity (V_{max}) of hydrolysis of clavulanic acid for each enzyme and was therefore used to calculate the k_{cat}. The turnover values (k_{cat}) obtained were 3.50 ± 0.01 s^{-1} for CRH-1 and 11.60 ± 0.01 s^{-1} for KPC-2, meaning that CRH-1 hydrolyzes clavulanic acid but at a lower rate than KPC-2.

Based on these results, we propose that the interaction between CRH-1 and clavulanic acid could follow a similar branched-pathway model previously proposed for KPC-2 (20). Once the active site is acylated by the inhibitor, it could lead to the formation of the totally inactivated enzyme (with possible rearrangement intermediates) or, alternatively, a fraction of the acylated enzyme could follow a hydrolytic pathway where the inhibitor is cleaved and inactivated. The fact that CRH-1 has a higher affinity and inactivation rate, with lower a hydrolytic rate than KPC-2, may suggest that the inactivation pathway is more favored than the hydrolytic one, leading to a 10-fold higher inhibition efficiency for CRH-1. However, although the hydrolytic rate is lower, it is enough to produce an overall weak inhibition by clavulanic acid.

Regarding inhibition by AVI, CRH-1 seems to have lower affinity for this inhibitor than KPC-2 ($K_{i\text{-app}}$ value 6.6-fold higher) (Table 3). Comparative acylation rate values (k_2/K) showed that CRH-1 exhibits a slightly higher k_2/K than KPC-2. These results demonstrate that both CRH-1 and KPC-2 are effectively inhibited by this DBO inhibitor, which correlates with the low MIC values of the combination CAZ/AVI for recombinant clones producing each enzyme. However, as these data do not clarify whether CRH-1 inhibition by avibactam

TABLE 4 X-ray data collection and refinement statistics

Crystal	Apo CRH-1	CRH-1/AVI
PDB code	8EHU	8EK9
Data collection		
Wavelength (Å)	0. 885601	0. 885601
Space group	$P\,2_1$	$P\,2_1$
Unit cell parameters		
a, b, c (Å)	36.43, 72.90, 52.06	36.50, 73.79, 51.53
α, β, γ (°)	90, 92.27, 90	90, 92.64, 90
Subunits/asymmetric unit	1	1
Resolution range (Å)[a]	42.34–1.10 (1.17–1.10)	42.22–1.40 (1.48–1.40)
Total reflections	725,689 (98,797)[a]	367,693 (58,468)[a]
Unique reflections	105,857 (16,478)[a]	53,514 (8,539)[a]
Redundancy	6.85	6.87
Completeness (%)	96.2 (92.9)[a]	99.6 (98.9)[a]
Mean I/σ(I)	22.61 (7.77)[a]	24.24 (1.76)[a]
Overall Wilson *B* factor (Å^2)	11	24
R_{meas}	0.052 (0.197)[a]	0.033 (1.007)[a]
CC (1/2)	0.998 (0.986)[a]	1.000 (0.814)[a]
Refinement		
Reflections used in refinement	105,817 (10,197)[a]	53,504 (5,282)[a]
R_{free} test set (%)	5,293 (5.0)[a]	2,675 (5.0)[a]
R_{work}	0.165	0.195
R_{free}	0.179	0.219
No. of nonhydrogen atoms	2,588	2,280
Macromolecules	2,019	1,991
Ligands	0	17
Solvent	569	272
Protein residues	270	266
RMS[b] deviations from ideal stereochemistry		
Bonds (Å)	0.008	0.010
Angles (°)	1.08	1.21
Avg *B*-factor (Å^2)		
All atoms	15	32
Protein	13	31
Ligand		31
Solvent	25	39
Ramachandran plot (%):		
Favored regions	97.8	97.7
Allowed regions	2.2	2.3
Outlier regions	0.00	0.00
Rotamer outliers (%)	0.49	0.99

[a]Statistics for the highest resolution shell are given in parentheses.
[b]RMS, root-mean square.

follows the same two-step hydrolytic pathway proposed for KPC-2 (shown in Fig. 1) (3), further studies should be performed to evaluate this inhibition mechanism.

Structural analysis of CRH-1 and its complex with avibactam. The crystal structure of the apo form of CRH-1 and its covalent complex with AVI were obtained at resolutions of 1.10 and 1.40 Å, respectively. Data collection and refinement statistics are given in Table 4. Both structures contained only one monomer per asymmetric unit, and the electron density map was well defined along the main chain in both cases. The amino acid numbering scheme used in this structure follows the Ambler consensus system (28). The protein chains for apo CRH-1 and the CRH-1/AVI complex include 270 (Ala24-Lys293) and 266 (Ser28-Lys293) residues, respectively. The structures were solvated by 569 (apo form) and 272 (AVI complex) ordered water molecules. The average root-mean-square deviation (RMSD) value for Cα atoms between the main chains of CRH-1 and its complex with AVI is 0.32 Å.

TABLE 5 Root-mean square deviations and percentage of amino acid identity between CRH-1 and other class A β-lactamases[a,b]

	RMSD (Å) (%) for:					
β-lactamase	CRH-1	KPC-2	SFC-1	CTX-M-15	Per-2	L2
CRH-1		0.63 (73.7)	0.87 (68.3)	0.92 (48.3)	1.89 (31.1)	1.23 (45.8)
KPC-2			0.70 (68.7)	0.87 (49.8)	1.82 (28.1)	1.24 (43.2)
SFC-1				0.94 (48.6)	1.83 (27.3)	1.27 (45.1)
CTX-M-15					1.86 (27.9)	1.20 (46.9)
PER-2						1.71 (27.4)

[a]PDB codes: KPC-2, 2OV5; SFC-1, 4EQI; CTX-M-15, 4HBT; PER-2, 6DGU; L2, 1N4O.
[b]Amino acid identity % corresponded to the aligned residues from the PDB structures.

The overall fold of the apo CRH-1 β-lactamase is similar to that of previously reported class A β-lactamases, and its catalytic cleft is also located in the junction between the main "all α" and "α/β" domains (29). The root-mean-square deviation (RMSD) values for Cα atoms between the main chain of CRH-1 and other class A β-lactamases were determined (Table 5). These values are consistent with the closer amino acid identity between CRH-1 and KPC and SFC-1 carbapenemases (30). Figure 2a shows the overall structure of CRH-1, which was superimposed with KPC-2 to visualize the high degree of structure conservation.

Like other class A β-lactamases, the active site motifs in CRH-1 are located in the interface between the all α and α/β domains. The active site is defined as Ser70-Ser71-Phe72-Lys73 (motif 1, carrying the nucleophilic serine residues), Ser130-Asp131-Asn132 (motif 2, in the loop between α4 and α5), Lys234-Thr235-Gly236 (motif 3, on strand β3), and the 16-residue-long Ω-loop, from Arg164 to Asp179 (Fig. 2b). The active site includes the most important amino acid residues located at conserved positions in class A β-lactamases, and all together create the hydrogen bond network for stabilization of the catalytic pocket. Unfortunately, the deacylating water is not clearly visible due to the packing of the crystal, and the N terminus of the neighboring molecule in the adjacent asymmetric unit lies just facing the active site entrance.

Analysis of the CRH-1/AVI complex demonstrates that AVI is covalently bound to the Ser70-O^{γ} atom and that the C7-N6 bond has been cleaved, for which cleavage of the C7-N1 bond is unlikely. This agrees with other structures with bound AVI (31, 32). Due to the high resolution obtained in the X-ray diffraction experiment, the defined $2mF_o$-DF_c electron density map can be clearly contoured around the amino acid residues and the AVI molecule (Fig. 3a). As observed in other AVI complexes, the 6-membered DBO ring adopts a chair conformation, stabilized by hydrogen bonds between (i) the C7-carbonyl of the newly formed carbamate and the backbone nitrogen atoms of Ser70 and Ser237 in the oxyanion hole and the deacylating water (DAW); (ii) the AVI amide moiety at C2 and Asn132-$N^{\delta 2}$ and water molecules; (iii) the AVI sulfate group

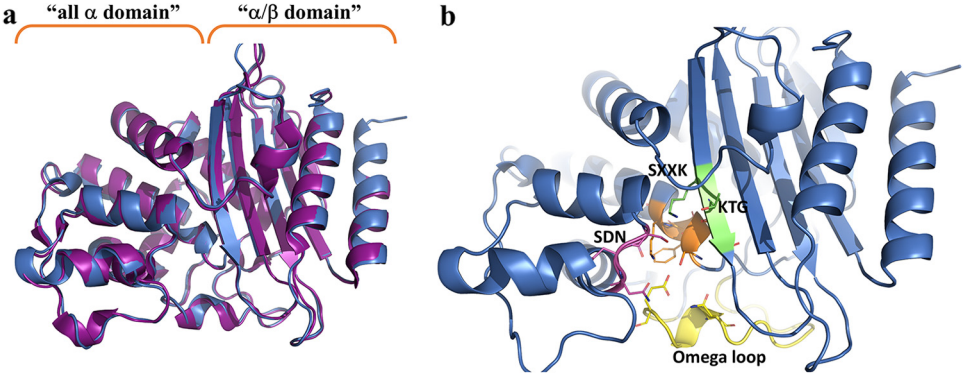

FIG 2 (a) Overall structure of superimposed structures of CRH-1 (blue) and KPC-2 (purple), indicating the spatial location of the all α and α/β domains. (b) Location of the conserved motifs and domains of CRH-1 that are involved in the architecture of the active site: SXXK motif (orange), SDN motif (magenta), KTG motif (green), and the Ω loop (yellow).

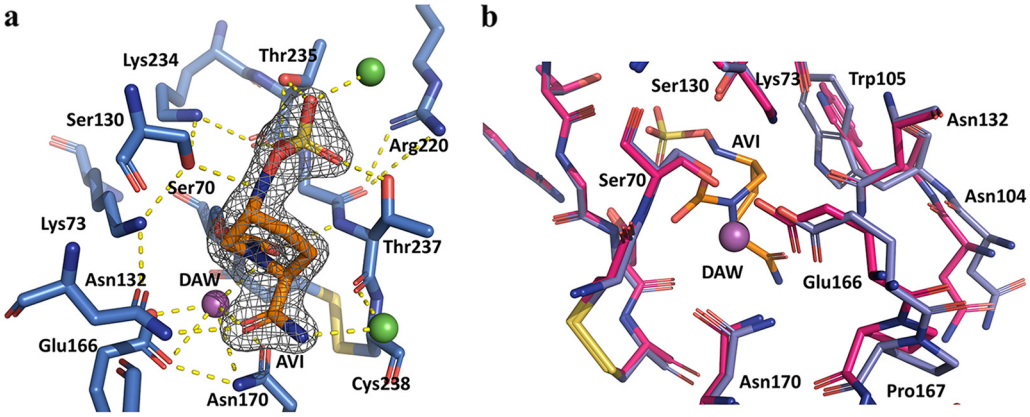

FIG 3 (a) Detail of the interaction of avibactam (orange sticks) in the active site of CRH-1, showing the $2mF_0 - DF_c$ electron density map contoured at 2 σ around the ligand (gray mesh); the purple sphere depicts the deacylating water (DAW); green spheres represent other water molecules involved in hydrogen bonds with AVI. (b) Main structural displacements and shifts observed upon AVI binding; apo CRH-1 is shown in pink tones, and the DAW molecule in this structure is depicted as a purple sphere.

and Thr235-O, Thr235-O$^{\gamma}$, Thr237-O$^{\gamma}$, and water molecules; and (iv) AVI-N6 with both Ser70-O$^{\gamma}$ and Ser130-O$^{\gamma}$. Additional interactions seem to contribute to the proper docking of AVI within the active site, creating second-shell hydrogen bonds: Asn170 and Glu166 through the DAW molecule, Lys73 through Ser70 and Ser130, Arg220 via Thr237, and Thr216 through likely conserved water molecules.

Upon binding of AVI, the side chains of Glu166 (0.8 Å) and Asn170 (0.65 Å) were shifted to create the proper hydrogen bonding network, probably due to a displacement of the deacylating water out of Ser70-Oγ. Other residues, mainly from the Ω loop (Pro167, Glu168), are also displaced due to AVI binding. Also, binding of AVI could allow a more favorable environment for creating hydrophobic interactions (likely π-π stacking) between Trp105 and the 6-membered AVI ring, as the side chain of this residue is oriented toward the DBO (Fig. 3b). Finally, the side chain of Lys73 points toward Ser130, which was associated with the proper orientation and activation of the deacylating water during catalysis (31).

The CRH-1/AVI complex structure was compared by superposition to other class A β-lactamases: CTX-M-15 (PDB 4HBU), KPC-2 (PDB 4ZBE), and PER-2 (PDB 6D3G). It was observed that the position and spatial arrangement of AVI within the active site is overall conserved in all compared structures (Fig. 4). The orientation of the sulfate moiety is

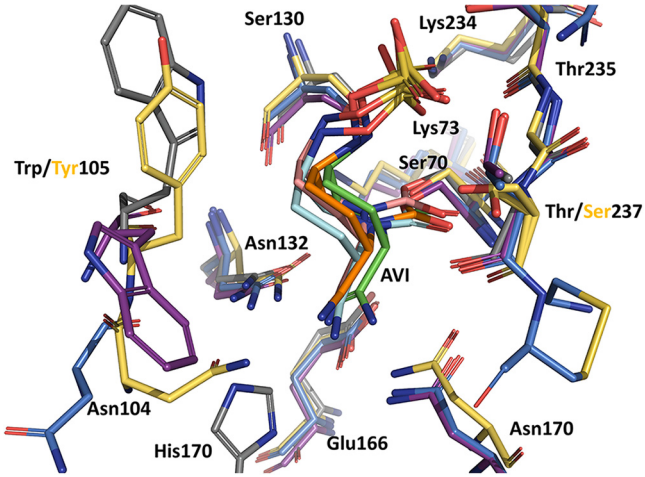

FIG 4 View of the active site of selected class A β-lactamases showing the main structural perturbations upon AVI binding. Color codes: blue/orange, CRH-1/AVI; yellow/green, CTX-M-15/AVI; purple/cyan, KPC-2/AVI; gray/pink, PER-2/AVI. Residues in yellow are only present in CTX-M-15.

more conserved between CRH-1 and CTX-M-15, although in the latter enzyme there is an additional hydrogen bond with Asn104, which together with the presence of an apparent less hydrophobic environment (Tyr105 in CTX-M-15 in place of Trp105 for the other three β-lactamases) can be associated with differences in AVI inhibition efficiency for different β-lactamases.

Conclusions. Our findings reveal that the hydrolytic behavior of CRH-1 β-lactamase toward penicillins, cephalosporins, and carbapenems is similar to that of KPC-2. Likewise, the propensity of CRH-1 to be inhibited by avibactam but not by clavulanic acid is also shared with KPC-2. We attribute the ineffective inhibition of CRH-1 by clavulanic acid to its hydrolytic activity toward this β-lactamase inhibitor. This kinetic profile correlates with the MIC values reported in this work for CRH-1, demonstrating that when bla_{CRH-1} is expressed under an efficient promoter, the consequent production of this enzyme confers resistance to β-lactams. The observed structural similarities in the interaction of AVI between CRH-1 and other serine-β-lactamases support the clinical utility of DBO inhibitors if this carbapenemase variant were to emerge in pathogenic bacterial species.

C. haemolyticum was first described in 2008 (33) and is highly associated with aquatic environments (34–36). However, human infections caused by this microorganism have also been reported, some of them associated with previous exposure to water bodies (37–40). Antimicrobial susceptibility testing performed in previous studies for *C. haemolyticum* isolates (both clinical and environmental) classified them all as susceptible to carbapenems (33, 37–39). The *C. haemolyticum* DSM19808 strain from which the CRH-1 gene used in our work was amplified was also susceptible to imipenem and meropenem. These are interesting findings because the CRH-encoding gene was found with a similar genetic context in all genomes available for this species (41). Additionally, three genes encoding putative β-lactamases of classes A, C, and D were also identified in these genomes (41).

These findings, along with the results presented in our study, reinforce the hypothesis that environmental microorganisms harbor genes that can confer a resistance phenotype when regulated by efficient expression systems. Particularly for CRH-1, although its carbapenemase activity was detected in the isolate of *C. haemolyticum* DSM19808 (17), it is likely that the expression of this *bla* gene is not sufficient to confer resistance to carbapenems in this species. Moreover, we could not attribute this carbapenemase activity to CRH-1 alone because of the possible concomitant production of other β-lactamases.

The amino acid identity between CRH-1 and KPC-2 is not high enough to propose this β-lactamase as the direct evolutionary origin of KPC-2. Nevertheless, the biochemical and structural similarities between both enzymes support the hypothesis that different carbapenemases could exist in the core genome of species closely related to the genus *Chromobacterium* which could act as reservoirs in the evolutionary pathway of KPC and related enzymes.

Analysis of *C. haemolyticum* genomes showed that no mobilization elements were identified in the regions flanking the CRH coding sequence that might indicate recruitment of this carbapenemase from the environmental resistome (17, 41). If CRH-1 is eventually recruited from the *C. haemolyticum* genome by a mobilization event, the favorable interactions observed with avibactam foresee an optimistic treatment scenario in case this type of enzyme emerges among clinical pathogens in the future.

MATERIALS AND METHODS

Bacterial strains and plasmids. The KPC-2 gene was recovered from a clinical *Klebsiella pneumoniae* strain previously characterized in our laboratory (42). A CRH-1-producing *Escherichia coli* recombinant clone was kindly provided by the authors of reference 17. *E. coli* TOP10 F′ (Invitrogen, USA) and *E. coli* BL21(DE3) (Novagen, Germany) were used as hosts for transformation experiments to obtain recombinant clones for antimicrobial susceptibility and overexpression assays, respectively. *Escherichia coli* ATCC 25922 and ATCC 35218 were used as control strains for antimicrobial susceptibility assays.

Plasmid vectors pGEM-T Easy Vector (Promega, USA) and pMBLe (43) were used for general cloning assays, and pET24a(+) (Novagen, Germany) was used for overproduction of both β-lactamases.

Recombinant DNA methodology. The complete *bla* genes were amplified from whole DNA of the corresponding strain by PCR using primers designed to introduce the NdeI and EcoRI restriction sites: KPC-F-NdeI (5-′CATATGTCACTGTATCGCC-3′) and KPC-R-EcoRI (5′-GAATTCTTACTGCCCGTT-3′), CRH-F-NdeI

(5′-CATATGTTCAAGCATCTG-3′) and CRH-R-EcoRI (5′-GAATTCTTATTTCTTCACG-3′) for KPC-2 and CRH-1, respectively. A proofreading *pfu* polymerase (Thermo Scientific, USA) was used in PCRs to avoid errors in the *bla* gene amplification. Amplified and purified amplicons were cloned into a pGEM-T Easy Vector (Promega, USA), and the resulting constructions were transformed into chemically competent *E. coli* TOP10F′ cells. The presence of the inserts and restriction sites was verified by DNA sequencing (Macrogen, South Korea). For subsequent clonings, the KPC-2 and CRH-1 genes were digested from the original construction, and the released fragments were purified and then ligated in the NdeI and EcoRI sites of pMBLe and pET24a(+) digested vectors. Ligation mixtures were transformed in chemically competent *E. coli* TOP10F′ cells, and recombinant clones were selected in lysogeny broth (LB) agar supplemented with 20 μg/mL gentamicin or 30 μg/mL kanamycin, depending on whether the constructions were obtained in pMBLe or pET24a(+) vectors, respectively. Recombinant plasmids of the selected clones were extracted and sequenced to verify the identity of *bla* genes and their proper insertion.

Antimicrobial susceptibility testing. MICs of different β-lactams and combinations with β-lactamase inhibitors were determined by the broth microdilution method according to the CLSI guidelines (44). For *E. coli* recombinant clones harboring the pMBLe/bla_{CRH-1} and pMBLe/bla_{KPC-2}, constructions were named pM-CRH-1 and pM-KPC-2, respectively. Gene expression in the pMBLe system is regulated by isopropyl-β-D-thiogalactoside (IPTG) induction (43), for which antimicrobial susceptibility assays were performed using LB supplemented with 50 μM IPTG. Mueller-Hinton broth was replaced by LB broth because suboptimal cell growth of recombinant clones in the first medium was achieved, preventing accurate MIC determinations.

MIC determinations for the environmental *Chromobacterium haemolyticum* DSM19808 strain were determined with the Sensititre system for MIC (Thermo Fisher, USA).

To assess whether CRH-1 is also inhibited by boronic acid in disk diffusion assays (which is a known behavior in KPC), we performed the double-disk diffusion synergy test (DDST) as previously described (18), with the modification of supplementing the medium with 50 μM IPTG.

Enzyme overproduction and purification. The KPC-2 and CRH-1 purification strategies were designed to purify both β-lactamases in their native state. Recombinant plasmids pET24a(+)/*bla* were transformed into *E. coli* BL21(DE3), and recombinant clones were selected with 30 μg/mL kanamycin. Overnight cultures of recombinant *E. coli* BL21(DE3) producing either CRH-1 or KPC-2 were diluted (1/50) in LB supplemented with 30 μg/mL kanamycin and incubated at 37°C until reaching an optical density (OD) of 0.7 to 0.8 at 600 nm. The overproduction of β-lactamases was induced with the addition of 0.5 mM IPTG. The induction conditions were optimized for each enzyme: KPC-2 expression was achieved at 37°C for 3 h, and CRH-1 induction was carried out at 25°C for 18 h, both with mechanical stirring (180 rpm).

After induction, cultures were harvested by centrifugation (8,000 rpm for 30 min at 4°C), pellets were resuspended with 50 mM sodium phosphate buffer, pH 7.0, and cell disruption was achieved by sonication. The obtained crude extracts were centrifuged at 13,000 rpm for 30 min at 4°C, and supernatants were then dialyzed overnight against buffer A (KPC-2: 20 mM sodium acetate buffer, pH 5.0; CRH-1: 50 mM sodium phosphate buffer, pH 7.0) with at least three changes of dialysis buffer. After filtration through 0.45-mm-pore-size membranes, clear and equilibrated supernatants were loaded onto a 5-mL HiTrap SP high-performance (HP) column (GE Healthcare Life Sciences, USA) preequilibrated with corresponding buffer A. Bound proteins were eluted with a continuous gradient (0% to 100%) of buffer B (buffer A supplemented with 1 M NaCl), and the collected fractions were analyzed by SDS-PAGE in 15% polyacrylamide gels. β-Lactamase activity was tested in all fractions by nitrocefin hydrolysis. Generally, one step of cation exchange chromatography was enough to obtain fractions of the purified protein of interest with purity of >90%, which was estimated by Coomassie blue staining on 15% polyacrylamide gels. According to the Lambert-Beer law, the protein concentration was determined by UV absorbance at 280 nm. The fractions of the purified enzymes were stored at −80°C for subsequent kinetics and crystallographic assays.

Kinetics. Steady-state kinetic parameters were determined using a T80 UV/Vis spectrophotometer (PG Instruments Ltd., UK). Each reaction was performed in a total volume of 500 μL at room temperature in 50 mM sodium phosphate buffer, pH 7.0. The steady-state kinetic parameters K_m and V_{max} for different β-lactams were obtained under an initial rate as described previously (45), with nonlinear least-squares fitting of the data (Henri Michaelis-Menten equation) using Prism 5.03 for Windows (GraphPad Software, USA) according to equation 1:

$$V = (V_{max} \times [S])/(K_m + [S]) \quad (1)$$

For low K_m values, the k_{cat} values were derived by the evaluation of the complete hydrolysis time courses as described by De Meester et al. (46). For poor substrates behaving as competitive inhibitors, the inhibition constant K_i (as $K_{i\text{-obs}}$) was determined by monitoring the residual activity of the enzyme in the presence of various concentrations of the antibiotic and nitrocefin as the reporter substrate (at a fixed concentration of five times the K_m for nitrocefin); the corrected K_i value (considered apparent K_m) was finally determined using equation 2:

$$K_i = K_{i-obs}/\left(1 + [NCF]/K_{m(NCF)}\right) \quad (2)$$

where $K_{m(NCF)}$ and [NCF] are the reporter substrate's K_m and fixed concentration used, respectively.

For high K_m values, V_{max} could not be reached because initial hydrolysis velocities did not approach enzyme saturation at testable concentrations. In these cases, the slope of the line obtained in the initial velocity versus antibiotic concentration plot was considered the second-order rate constant for

hydrolysis at steady state (k_{cat}/K_m), and K_m values were determined as inhibition constant K_i in competitive assays with nitrocefin as the reporter substrate.

The interaction of KPC-2 with AVI was proposed to follow the equation presented in Fig. 1. Unlike other class A β-lactamases, this mechanism proposes that after the KPC-2 active site is acylated by AVI, a slow two-step hydrolytic pathway occurs, leading to the deacylated enzyme (3). The formation of the noncovalent complex E:I is represented by K_i (equivalent to k_{-1}/k_1). For β-lactamases that acylate very slowly, apparent K_i (K_{i-app}) values can approximate the K_i of the inhibitor; otherwise, for β-lactamases with a fast acylation rate, the K_{i-app} approximates the K_m of the enzyme for the inhibitor. The inhibition constant K_{i-app}s were determined as reported previously (3, 4, 47) using a direct competition assay under steady-state conditions with nitrocefin as the reporter substrate. Initial velocities (V_0) were determined after mixing nitrocefin (at a concentration of 5 times the K_m for this substrate) with a fixed concentration of enzyme (kept at a nanomolar range) and increasing concentrations of avibactam. An inverse initial steady-state velocity ($1/V_0$) versus inhibitor concentration (I) plot was obtained, and the K_{i-app} observed was calculated by dividing the value of the *y*-intercept by the slope of the line. K_{i-app} values were then corrected using equation 3:

$$K_{\mathrm{i-app}}(\mathrm{corrected}) = K_{i-\mathrm{app}}(\mathrm{observed})/(1 + ([\mathrm{S}]/K_{m(NCF)})) \quad (3)$$

For the determination of the acylation rate (k_2/K), progress curves were obtained under the same conditions previously mentioned for the K_{i-app} determination and then fitted to equation 4 to calculate k_{obs} values using a nonlinear least-squares method with Prism 5.03 for Windows (GraphPad Software, USA):

$$y = V_f \times t + (V_0 - V_f) \times (1 - e^{-k_{\mathrm{obs}}})/k_{\mathrm{obs}} + \mathrm{A}_0 \quad (4)$$

For equation 4, V_f is the final velocity, V_0 is the initial velocity, t is time and A_0 is the initial absorbance at λ = 482 nm. The data were plotted as k_{obs} versus [I], and then k_2/K observed was calculated from the slope of the line according to equation 5, where [I] is the concentration of AVI, [S] is the concentration of nitrocefin, and k_{-2} is the recyclization rate constant:

$$k_{\mathrm{obs}} = k_{-2} + (k_2/K_{\mathrm{obs}}) \times [\mathrm{I}]/\left(1 + \left([\mathrm{S}]/K_{m(NCF)}\right)\right) \quad (5)$$

Finally, the k_2/K value was obtained by correcting the k_2/K_{obs} value considering the concentration and affinity of nitrocefin (equation 6):

$$k_2/K = k_2/K_{\mathrm{obs}} \times \left(1 + \left([\mathrm{S}]/K_{m(NCF)}\right)\right) \quad (6)$$

Previous studies demonstrated that KPC-2 can hydrolyze clavulanic acid (19, 20). To assess whether CRH-1 shares the same behavior, K_m and k_{inact} values for clavulanic acid of KPC-2 and CRH-1 were determined as previously reported by Papp-Wallace et al. (19, 20). The initial velocity (V_0) of clavulanic acid hydrolysis was monitored at 235 nm (19), mixing an inhibitor concentration 5 times the K_m determined and 100 nM enzyme. The V_0 obtained under this condition was considered the V_{max} and was used to determine the k_{cat} for clavulanic acid.

The following extinction coefficients and wavelengths were used: ampicillin ($\Delta\varepsilon_{235}$, -820 M^{-1} cm^{-1}), piperacillin ($\Delta\varepsilon_{235}$, -820 M^{-1} cm^{-1}), cephalothin ($\Delta\varepsilon_{273}$, $-6{,}300$ M^{-1} cm^{-1}), ceftriaxone ($\Delta\varepsilon_{260}$, $-9{,}400$ M^{-1} cm^{-1}), ceftazidime ($\Delta\varepsilon_{260}$, $-7{,}500$ M^{-1} cm^{-1}), cefepime ($\Delta\varepsilon_{260}$, $-10{,}000$ M^{-1} cm^{-1}), aztreonam ($\Delta\varepsilon_{318}$, -750 M^{-1} cm^{-1}), imipenem ($\Delta\varepsilon_{300}$, $-9{,}000$ M^{-1} cm^{-1}), meropenem ($\Delta\varepsilon_{300}$, $-6{,}500$ M^{-1} cm^{-1}), clavulanic acid ($\Delta\varepsilon_{2350}$, $-1{,}630$ M^{-1} cm^{-1}), and nitrocefin ($\Delta\varepsilon_{482}$, $+15{,}000$ M^{-1} cm^{-1}).

Crystallization of apo and AVI-bound CRH-1. Crystals of apo CRH-1 were grown by the hanging drop vapor diffusion method (20°C) with drops containing 2 μL of enzyme solution (20 mg/mL) and 2 μL of crystallization solution consisting of 18% (wt/vol) polyethylene glycol (PEG) 4000, 0.2 M lithium chloride, and 0.1 M Tris-HCl buffer, pH 8.5. For the adduct structure with AVI, we used crystals obtained by equivalent conditions in 22% (wt/vol) PEG 4000, 0.2 M lithium chloride, and 0.1 M Tris-HCl buffer, pH 7.6; then, the crystals were soaked in the crystallization solution supplemented with 100 mM AVI for 24 h. All samples were cryoprotected in mother liquor supplemented with 15% (wt/vol) PEG 400 and then flash-cooled in liquid nitrogen in Hampton Research loops (Aliso Viejo, CA, USA).

Data collection, phasing, model building, and refinement. Native X-ray diffraction data were collected at 100 K at the PROXIMA 2A beamline at the SOLEIL Synchrotron (Saint Aubin, France), using a Dectris EIGER X 9M detector (Baden, Switzerland). Integration and scaling were carried out using XDS (48). Structure resolution was achieved by molecular replacement through Phaser (49), using the *Serratia fonticola* SFC-1 carbapenemase structure (PDB 4EQI) as the starting model (50). Refinement and model building were performed with PHENIX 1.12-2829 (51) and Coot 0.8.6.1 (Turtle Bay) (52), respectively. Models were validated with MolProbity (53) and visualized with PyMOL 1.7.0.3 (54).

Data availability. The coordinates and structure factor amplitudes of apo CRH-1 and the CRH-1/AVI complex were deposited at the Protein Data Bank under accession codes 8EHU and 8EK9, respectively.

ACKNOWLEDGMENTS

This research was funded in part by grants from the University of Buenos Aires (UBACyT 2018 20020170100072BA to P.P.), Agencia Nacional de Promoción Científica y Tecnológica (BID PICT 2018-01550 to P.P.), and Consejo Nacional de Investigaciones

Científicas y Técnicas (PIP 11220200100191CO to P.P.). These grants were received in local currency (Argentinean pesos) and do not cover APC.

The authors acknowledge access to the PROXIMA 2A beamline at the SOLEIL Synchrotron, France (proposal no. 20181069).

This work was partially supported by iNEXT-Discovery, project no. 871037, PID 17062, funded by the Horizon 2020 program of the European Commission.

P.P., B.G., S.K., and G.G. are researchers at the Consejo Nacional de Investigaciones Científicas y Técnicas (CONICET, Argentina).

We declare no conflict of interest.

REFERENCES

1. van Duin D, Doi Y. 2017. The global epidemiology of carbapenemase-producing Enterobacteriaceae. Virulence 8:460–469. https://doi.org/10.1080/21505594.2016.1222343.
2. Lee C-R, Lee JH, Park KS, Kim YB, Jeong BC, Lee SH. 2016. Global dissemination of carbapenemase-producing Klebsiella pneumoniae: epidemiology, genetic context, treatment options, and detection methods. Front Microbiol 7:895. https://doi.org/10.3389/fmicb.2016.00895.
3. Ehmann DE, Jahić H, Ross PL, Gu R-F, Hu J, Durand-Réville TF, Lahiri S, Thresher J, Livchak S, Gao N, Palmer T, Walkup GK, Fisher SL. 2013. Kinetics of avibactam inhibition against Class A, C, and D β-lactamases. J Biol Chem 288:27960–27971.1. https://doi.org/10.1074/jbc.M113.485979.
4. Ehmann DE, Jahić H, Ross PL, Gu R-F, Hu J, Kern G, Walkup GK, Fisher SL. 2012. Avibactam is a covalent, reversible, non–β-lactam β-lactamase inhibitor. Proc Natl Acad Sci U S A 109:11663–11668.1. https://doi.org/10.1073/pnas.1205073109.
5. Shields RK, Nguyen MH, Chen L, Press EG, Potoski BA, Marini RV, Doi Y, Kreiswirth BN, Clancy CJ. 2017. Ceftazidime-avibactam is superior to other treatment regimens against carbapenem-resistant Klebsiella pneumoniae bacteremia. Antimicrob Agents Chemother 61:e00883-17. https://doi.org/10.1128/AAC.00883-17.
6. Castanheira M, Mills JC, Costello SE, Jones RN, Sader HS. 2015. Ceftazidime-avibactam activity tested against Enterobacteriaceae isolates from U.S. Hospitals (2011 to 2013) and characterization of β-lactamase-producing strains. Antimicrob Agents Chemother 59:3509–3517. https://doi.org/10.1128/AAC.00163-15.
7. Galán J-C, González-Candelas F, Rolain J-M, Cantón R. 2013. Antibiotics as selectors and accelerators of diversity in the mechanisms of resistance: from the resistome to genetic plasticity in the β-lactamases world. Front Microbiol 4:9. https://doi.org/10.3389/fmicb.2013.00009.
8. Bush K. 2018. Past and present perspectives on β-lactamases. Antimicrob Agents Chemother 62:e01076-18. https://doi.org/10.1128/AAC.01076-18.
9. Martínez JL, Coque TM, Baquero F. 2015. What is a resistance gene? Ranking risk in resistomes. Nat Rev Microbiol 13:116–123. https://doi.org/10.1038/nrmicro3399.
10. D'Costa VM, McGrann KM, Hughes DW, Wright GD. 2006. Sampling the antibiotic resistome. Science 311:374–377. https://doi.org/10.1126/science.1120800.
11. Wright GD. 2010. The antibiotic resistome. Expert Opin Drug Discov 5:779–788. https://doi.org/10.1517/17460441.2010.497535.
12. Olson AB, Silverman M, Boyd DA, McGeer A, Willey BM, Pong-Porter V, Daneman N, Mulvey MR. 2005. Identification of a progenitor of the CTX-M-9 group of extended-spectrum β-lactamases from Kluyvera georgiana isolated in Guyana. 49:4. https://doi.org/10.1128/AAC.49.5.2112-2115.2005.
13. Rodríguez MM, Power P, Radice M, Vay C, Famiglietti A, Galleni M, Ayala JA, Gutkind G. 2004. Chromosome-encoded CTX-M-3 from Kluyvera ascorbata: a possible origin of plasmid-borne CTX-M-1-derived cefotaximases. Antimicrob Agents Chemother 48:4895–4897. https://doi.org/10.1128/AAC.48.12.4895-4897.2004.
14. Poirel L, Kampfer P, Nordmann P. 2002. Chromosome-encoded ambler class A β-lactamase of Kluyvera georgiana, a probable progenitor of a subgroup of CTX-M extended-spectrum β-lactamases. Antimicrob Agents Chemother 46:4038–4040. https://doi.org/10.1128/AAC.46.12.4038-4040.2002.
15. Humeniuk C, Arlet G, Gautier V, Grimont P, Labia R, Philippon A. 2002. β-Lactamases of Kluyvera ascorbata, probable progenitors of some plasmid-encoded CTX-M types. Antimicrob Agents Chemother 46:3045–3049. https://doi.org/10.1128/AAC.46.9.3045-3049.2002.
16. Ebmeyer S, Kristiansson E, Larsson DGJ. 2019. PER extended-spectrum β-lactamases originate from Pararheinheimera spp. Int J Antimicrob Agents 53:158–164. https://doi.org/10.1016/j.ijantimicag.2018.10.019.
17. Gudeta DD, Bortolaia V, Jayol A, Poirel L, Nordmann P, Guardabassi L. 2016. Chromobacterium spp. harbour Ambler class A β-lactamases showing high identity with KPC. J Antimicrob Chemother 71:1493–1496. https://doi.org/10.1093/jac/dkw020.
18. Pasteran F, Mendez T, Guerriero L, Rapoport M, Corso A. 2009. Sensitive screening tests for suspected class A carbapenemase production in species of Enterobacteriaceae. J Clin Microbiol 47:1631–1639. https://doi.org/10.1128/JCM.00130-09.
19. Papp-Wallace KM, Taracila MA, Smith KM, Xu Y, Bonomo RA. 2012. Understanding the molecular determinants of substrate and inhibitor specificities in the carbapenemase KPC-2: exploring the roles of Arg220 and Glu276. Antimicrob Agents Chemother 56:4428–4438. https://doi.org/10.1128/AAC.05769-11.
20. Papp-Wallace KM, Bethel CR, Distler AM, Kasuboski C, Taracila M, Bonomo RA. 2010. Inhibitor resistance in the KPC-2 β-lactamase, a preeminent property of this class A β-lactamase. Antimicrob Agents Chemother 54:890–897. https://doi.org/10.1128/AAC.00693-09.
21. Ghiglione B, Rodríguez MM, Herman R, Curto L, Dropa M, Bouillenne F, Kerff F, Galleni M, Charlier P, Gutkind G, Sauvage E, Power P. 2015. Structural and kinetic insights into the "ceftazidimase" behavior of the extended-spectrum β-lactamase CTX-M-96. Biochemistry 54:5072–5082. https://doi.org/10.1021/acs.biochem.5b00313.
22. Ruggiero M, Curto L, Brunetti F, Sauvage E, Galleni M, Power P, Gutkind G. 2017. Impact of mutations at Arg220 and Thr237 in PER-2 β-lactamase on conformation, activity, and susceptibility to inhibitors. Antimicrob Agents Chemother 61:e02193-16. https://doi.org/10.1128/AAC.02193-16.
23. Queenan AM, Torres-Viera C, Gold HS, Carmeli Y, Eliopoulos GM, Moellering RC, Quinn JP, Hindler J, Medeiros AA, Bush K. 2000. SME-type carbapenem-hydrolyzing class A β-lactamases from geographically diverse Serratia marcescens strains. Antimicrob Agents Chemother 44:3035–3039. https://doi.org/10.1128/AAC.44.11.3035-3039.2000.
24. Rasmussen BA, Bush K, Keeney D, Yang Y, Hare R, O'Gara C, Medeiros AA. 1996. Characterization of IMI-1 beta-lactamase, a class a carbapenem-hydrolyzing enzyme from Enterobacter cloacae. Antimicrob Agents Chemother 40:2080–2086. https://doi.org/10.1128/AAC.40.9.2080.
25. Mariotte-Boyer S, Nicolas-Chanoine MH, Labia R. 1996. A kinetic study of NMC-A β-lactamase, an Ambler class A carbapenemase also hydrolyzing cephamycins. FEMS Microbiol Lett 143:29–33. https://doi.org/10.1111/j.1574-6968.1996.tb08457.x.
26. Girlich D, Poirel L, Nordmann P. 2010. Novel ambler class A carbapenem-hydrolyzing β-lactamase from a Pseudomonas fluorescens isolate from the Seine River, Paris, France. Antimicrob Agents Chemother 54:328–332. https://doi.org/10.1128/AAC.00961-09.
27. Fonseca F, Sarmento AC, Henriques I, Samyn B, van Beeumen J, Domingues P, Domingues MR, Saavedra MJ, Correia A. 2007. Biochemical characterization of SFC-1, a class A carbapenem-hydrolyzing β-lactamase. Antimicrob Agents Chemother 51:4512–4514. https://doi.org/10.1128/AAC.00491-07.
28. Ambler RP, Coulson AF, Frère JM, Ghuysen JM, Joris B, Forsman M, Levesque RC, Tiraby G, Waley SG. 1991. A standard numbering scheme for the class A beta-lactamases. Biochem J 276:269–270. https://doi.org/10.1042/bj2760269.
29. Ghuysen JM. 1991. Serine beta-lactamases and penicillin-binding proteins. Annu Rev Microbiol 45:37–67. https://doi.org/10.1146/annurev.mi.45.100191.000345.
30. Fonseca F, Chudyk EI, van der Kamp MW, Correia A, Mulholland AJ, Spencer J. 2012. The basis for carbapenem hydrolysis by class A β-lactamases: a combined investigation using crystallography and simulations. J Am Chem Soc 134:18275–18285. https://doi.org/10.1021/ja304460j.

31. Lahiri SD, Mangani S, Durand-Reville T, Benvenuti M, De Luca F, Sanyal G, Docquier JD. 2013. Structural insight into potent broad-spectrum inhibition with reversible recyclization mechanism: avibactam in complex with CTX-M-15 and Pseudomonas aeruginosa AmpC beta-lactamases. Antimicrob Agents Chemother 57:2496–2505. https://doi.org/10.1128/AAC.02247-12.
32. Ruggiero M, Papp-Wallace KM, Brunetti F, Barnes MD, Bonomo RA, Gutkind G, Klinke S, Power P. 2019. Structural insights into the inhibition of the extended-spectrum beta-lactamase PER-2 by avibactam. Antimicrob Agents Chemother 63:e00487-19. https://doi.org/10.1128/AAC.00487-19.
33. Han XY, Han FS, Segal J. 2008. Chromobacterium haemolyticum sp. nov., a strongly haemolytic species. Int J Syst Evol Microbiol 58:1398–1403. https://doi.org/10.1099/ijs.0.64681-0.
34. Lima-Bittencourt CI, Costa PS, Barbosa FAR, Chartone-Souza E, Nascimento AMA, Nascimento AMA. 2011. Characterization of a Chromobacterium haemolyticum population from a natural tropical lake. Lett Appl Microbiol 52:642–650. https://doi.org/10.1111/j.1472-765X.2011.03052.x.
35. Tacão M, Correia A, Henriques IS. 2015. Low prevalence of carbapenem-resistant bacteria in river water: resistance is mostly related to intrinsic mechanisms. Microb Drug Resist 21:497–506. https://doi.org/10.1089/mdr.2015.0072.
36. Priya K, Sulaiman J, How KY, Yin W-F, Chan K-G. 2018. Production of N-acyl homoserine lactones by Chromobacterium haemolyticum KM2 isolated from the river water in Malaysia. Arch Microbiol 200:1135–1142. https://doi.org/10.1007/s00203-018-1526-y.
37. Okada M, Inokuchi R, Shinohara K, Matsumoto A, Ono Y, Narita M, Narita M, Ishida T, Kazuki C, Nakajima S, Yahagi N. 2013. Chromobacterium haemolyticum-induced bacteremia in a healthy young man. BMC Infect Dis 13:406–406. https://doi.org/10.1186/1471-2334-13-406.
38. Takenaka R, Nureki S, Ueno T, Shigemitsu O, Miyazaki E, Kadota J, Miki T, Okada N. 2015. Chromobacterium haemolyticum Pneumonia Possibly Due to the Aspiration of Runoff Water. Jpn J Infect Dis 68:526–529. https://doi.org/10.7883/yoken.JJID.2014.285.
39. Harmon N, Mortensen JE, Robinette E, Powell EA. 2016. Pediatric bacteremia caused by Chromobacterium haemolyticum/Chromobacterium aquaticum. Diagn Microbiol Infect Dis 86:108–111. https://doi.org/10.1016/j.diagmicrobio.2016.05.021.
40. Tanpowpong P, Charoenmuang R, Apiwattanakul N. 2014. First pediatric case of Chromobacterium haemolyticum causing proctocolitis. Pediatr Int 56:615–617. https://doi.org/10.1111/ped.12301.
41. Teixeira P, Tacão M, Baraúna RA, Silva A, Henriques I. 2020. Genomic analysis of Chromobacterium haemolyticum: insights into the species resistome, virulence determinants and genome plasticity. Mol Genet Genomics 295:1001–1012. https://doi.org/10.1007/s00438-020-01676-8.
42. Cejas D, Fernandez Canigia L, Nastro M, Rodríguez C, Tanco A, Rodríguez H, Vay C, Maldonado I, Famiglietti A, Giovanakis M, Magariños F, Berardinelli E, Neira L, Mollerach M, Gutkind G, Radice M. 2012. Hyperendemic clone of KPC producing Klebsiella pneumoniae ST 258 in Buenos Aires hospitals. Infect Genet Evol 12:499–501. https://doi.org/10.1016/j.meegid.2011.09.018.
43. González LJ, Bahr G, Nakashige TG, Nolan EM, Bonomo RA, Vila AJ. 2016. Membrane anchoring stabilizes and favors secretion of New Delhi metallo-β-lactamase. Nat Chem Biol 12:516–522. https://doi.org/10.1038/nchembio.2083.
44. CLSI. 2022. Performance standards for antimicrobial susceptibility testing, 32nd ed. CLSI supplement M100. Clinical and Laboratory Standards Institute, Wayne, PA.
45. Segel IH. 1975. Enzyme kinetics, behavior and analysis of rapid equilibrium and steady-state enzyme systems. John Wiley & Sons, Inc., New York, NY.
46. De Meester F, Joris B, Reckinger G, Bellefroid-Bourguignon C, Frere JM, Waley SG. 1987. Automated analysis of enzyme inactivation phenomena: application to β-lactamases and DD-peptidases. Biochem Pharmacol 36:2393–2403. https://doi.org/10.1016/0006-2952(87)90609-5.
47. Papp-Wallace KM, Winkler ML, Taracila MA, Bonomo RA. 2015. Variants of β-lactamase KPC-2 that are resistant to inhibition by avibactam. Antimicrob Agents Chemother 59:3710–3717. https://doi.org/10.1128/AAC.04406-14.
48. Kabsch W. 2010. XDS. Acta Crystallogr D Biol Crystallogr 66:125–132. https://doi.org/10.1107/S0907444909047337.
49. McCoy AJ, Grosse-Kunstleve RW, Adams PD, Winn MD, Storoni LC, Read RJ. 2007. Phaser crystallographic software. J Appl Crystallogr 40:658–674. https://doi.org/10.1107/S0021889807021206.
50. Nichols DA, Hargis JC, Sanishvili R, Jaishankar P, Defrees K, Smith EW, Wang KK, Prati F, Renslo AR, Woodcock HL, Chen Y. 2015. Ligand-induced proton transfer and low-barrier hydrogen bond revealed by X-ray crystallography. J Am Chem Soc 137:8086–8095. https://doi.org/10.1021/jacs.5b00749.
51. Adams PD, Afonine PV, Bunkoczi G, Chen VB, Davis IW, Echols N, Headd JJ, Hung LW, Kapral GJ, Grosse-Kunstleve RW, McCoy AJ, Moriarty NW, Oeffner R, Read RJ, Richardson DC, Richardson JS, Terwilliger TC, Zwart PH. 2010. PHENIX: a comprehensive Python-based system for macromolecular structure solution. Acta Crystallogr D Biol Crystallogr 66:213–221. https://doi.org/10.1107/S0907444909052925.
52. Emsley P, Cowtan K. 2004. Coot: model-building tools for molecular graphics. Acta Crystallogr D Biol Crystallogr 60:2126–2132. https://doi.org/10.1107/S0907444904019158.
53. Chen VB, Arendall WB, Headd JJ, Keedy DA, Immormino RM, Kapral GJ, Murray LW, Richardson JS, Richardson DC. 2010. MolProbity: all-atom structure validation for macromolecular crystallography. Acta Crystallogr D Biol Crystallogr 66:12–21. https://doi.org/10.1107/S0907444909042073.
54. Schrödinger LLC. 2012. The PyMOL molecular graphics system. v2.0. https://pymol.org/2/#page-top.